Journal of Engineering Science and Technology
Vol. 13, No. 6 (2018) 1850 - 1868

PARAMETRIC IDENTIFICATION AND STABILIZATION OF TURBO-COMPRESSOR PLANT BASED ON MATRIX FRACTION DESCRIPTION USING EXPERIMENTAL DATA

BACHIR NAIL[1], ABDELLAH KOUZOU[1],
AHMED HAFAIFA[1,*], AHMED CHAIBET[2]

[1]The Applied Automation and Industrial Diagnostics Laboratory LAADI, Faculty of Science and Technology, University of DJELFA, Algeria
[2]Aeronautical Aerospace Automotive Railway Engineering school, ESTACA Paris, France
*Corresponding Author: a.hafaifa@univ-djelfa.dz

Abstract

This paper deals with the application of the multivariable linear system Matrix Fraction Description (MFD) theory for the identification of the Left Linear MIMO ARX turbo-compressor model based on Extended Least Square (ELS) estimator. Indeed, the identification of studied system model parameters is achieved using the experimental (inputs/outputs) data, which have been obtained by measurement on site where the main aim is to ensure the selection of the best model with minimum order. For the validation of the obtained results, a comparative study has been performed with the Hammerstein-Wiener model based on validation criteria where the reliability of the obtained model is taken into account. Finally, a right/left block solvent in several canonical forms have been assigned to present a comparative study, where the objective to ensure the stability enhancement of the dynamic behaviour of the studied turbo-compressor.

Keywords: ARX, Extended Least Square, Gas Turbo-compressor, Hammerstein-Wiener model, Linear system, Matrix Fraction Description (MFD), Solvents, Stability, System identification.

1. Introduction

The rotating machines used in oil & gas industrials are presenting the backbone of the whole production processes used in these important industrial plants. In this context, the centrifugal compressors that are among the vital rotating machines driven by gas turbines, whereas these machines are designed to operate continuously over a long period of time. A centrifugal compressor is a high-speed

Nomenclatures

A	Dynamic (system) matrix
B	Controllability matrix
C	Observability matrix
D	Coupling matrix
d	Number of estimated parameters
l	Number of blocks
m	Model inputs
n	Model order
N	Number of values in the estimation data set
$P1$	Aspiration pressure, kg/cm2
$P2$	Discharge pressure, kg/cm2
P	Model outputs
q^{-1}	Delay operator
R	Real numbers
T_1	Aspiration temperature, °C
T_2	Discharge temperature, °C
V	Loss function
x	State
y	Output signals
$\hat{y}$	Estimate output signals

Greek Symbols

θ	Matrix of parameters
Φ	Matrix of information

Abbreviations

ARX	Autoregressive with exogenous excitation
AIC	Information criteria
ELS	Information criteria
FPE	Final prediction error
LMFD	Left matrix fraction description
MFD	Matrix fraction description
MIMO	Multi inputs multi outputs
NLHW	Nonlinear Hammerstein-wiener model
RMSE	Normalized root mean squared error
VAF	Variance accounting for

rotating machine (approximately 6,000 to 30,000 rpm) in which one or more wheels provide the energy required to transfer the gas. When this energy has to be important, it is necessary to provide several wheels (multi-cellular), this sometimes leads to multi-stage machine solutions. The speed of rotation of the wheel subjects the gas to a centrifugal force, which results in an increase in speed, pressure and temperature in the wheel. The diffuser and the return channel allow to bring the gas back into the next wheel by gaining more pressure compared to that of the wheel outlet by slowing down the speed of the gas. Before applying any control law to the centrifugal compressor, it is important to find their mathematical model, which represent all the behaviour dynamics.

More recent research have been done and published along the recent years about the modelling and the stability of the centrifugal gas compressor dynamics such as the analytical model of centrifugal compressor validation based on experimental data [1], the turbulence model predictions assessment for an aero-engine centrifugal compressor [2], the prediction and measurement of centrifugal compressor axial forces during surge part 2 [3], the centrifugal compressor stability prediction using a new physics based approach [4], the analysis of the effects of pulsations on the operational stability of centrifugal compressors in mixed reciprocating and centrifugal compressor stations [5], the control of an ultrahigh-speed centrifugal compressor for the air management of fuel cell systems [6], the stability improvement of high-pressure-ratio turbocharger centrifugal compressor by asymmetric flow control in centrifugal compressor [7], and the design improvement of a high pressure casing with the help of finite element analysis to ensure the rotor dynamic stability of a high pressure centrifugal compressor equipped with a hole pattern seal [8].

The use of physical or mechanical laws is not always obviously, and is not the objective of this work. However the system identification presented in this paper focuses on the problem of obtaining "approximate" models of dynamic systems based on real measured input/output data, which is often sufficient to achieve control goals in advanced engineering application. The majority of the researches that have been done on modelling the gas turbo-compressor are mainly based on the artificial intelligence theory (Fuzzy Logic, ANFIS and Neural Network, etc.).

Among the disadvantages of these models are the control difficulty and the instability problem, furthermore, there are limitations of applying the advanced control theories due to the lack of the mathematical model. Indeed, there are many results that have been published in the recent years on the modelling of the gas turbo-compressor the and gas turbine such as the modelling of gas turbine based on fuzzy clustering algorithm via experimental data [9], the centrifugal compressor control and modelling used in gas transportation systems [10], the modelling of the centrifugal compressor using fuzzy logic [11], the adaptive control of centrifugal compressors [12], and others [13, 14]. On the other hand, the parametric system identification based on the estimation theory is the main tool which is used in this paper, where the main objective to find an approximate model that represents all the behaviour of the inputs/outputs signals of the studied gas turbo-compressor.

A recent paper has been published on MIMO system identification methods using the left and right matrix fraction description such as, optimal instrumental variable identification method for LMFD models [15], extending the SRIV algorithm to LMFD models [16], MIMO discrete-time systems identification using an observable canonical-form [17], and others [18, 19]. In the same time, there are many theories research that are focusing on the nonlinear systems parametric identification, as an example, the nonlinear ARX model and the parametric identification based on the Hammerstein-Wiener model, which produces a nonlinear model that will be used in this study as comparison example. Some interesting papers published in this area such as the nonlinear ARMAX Hammerstein systems identification [20], the parametric identification of parallel Hammerstein systems [21], the wiener Hammerstein system Identification based on the polynomial nonlinear state space algorithm [22], and others [23-25].

This work aims to identify and model the behaviour of gas turbo-compressor, which is installed in the natural gas field of Hassi R'Mel located at the south of

Algeria. The used parametric multivariable ARX model is obtained via the extended least square estimator based on Left matrix fraction description theory (LMFD) using experimental data, this multivariable model consists of two inputs, the aspiration temperature and pressure (T1, P1) and two outputs, the discharge temperature and pressure (T2, P2). The validity of the model order has been achieved with the checking of many criteria validations such as AIC/FPE and RMSE/VAF [26, 27]. In this paper to achieve the objective of ensuring the control and the stability of the dynamic behaviour, the block solvents placement based on the theory of the MFD has been applied [28, 29]. Furthermore, has been presented for the selection of the best form of the solvents in the left or right block Vandermonde.

The present paper is organized as follows: firstly, some preliminaries about Matrix Faction Description (MFD) are presented in the second section. The theory of extended Least Square based on MFD is presented in third section, whereas the fourth section introduces briefly the Hammerstein-Wiener model identification, and some validations criteria formulas. Finally, the last section presents the obtained results discussions and comments, the perspectives and a conclusion.

2. Matrix Fraction Description based method

Matrix Faction Description (MFD) is a representation of a matrix transfer function of a multivariable system as a ratio of two polynomial matrices. An introduction to matrix polynomials and MFD properties are given in [30-33]. The MFD approach is based on the fact that the Transfer Function Matrices and a MIMO system which can be described by the vector equation can be represented as ratio of two polynomial matrices.

$$y[k] = G(q^{-1})u[k] + H(q^{-1})e[k] \tag{1}$$

However, because matrices do not commute in general, it is noted that there are two representations for the transfer function matrix $G(q^{-1})$ or $H(q^{-1})$ as a ratio of two polynomial matrices, which are:

- Right Matrix Fraction Description (RMFD)

$$G(q^{-1}) = C(q^{-1})D^{-1}(q^{-1}) \tag{2}$$

- Left Matrix Fraction Description (LMFD)

$$G(q^{-1}) = A^{-1}(q^{-1})B(q^{-1}) \tag{3}$$

and $A^{-1}(q^{-1})$, $C(q^{-1})$ and $D(q^{-1})$ are matrix polynomials, which have the following structures:

$$\begin{cases} A(q^{-1}) = I_p + A_1 q^{-1} + \cdots + A_{na} q^{-na} \\ B(q^{-1}) = B_0 + B_1 q^{-1} + \cdots + B_{nb} q^{-nb} \\ C(q^{-1}) = C_0 + C_1 q^{-1} + \cdots + C_{nc} q^{-nc} \\ D(q^{-1}) = I_m + D_1 q^{-1} + \cdots + D_{nd} q^{-nd} \end{cases} \tag{4}$$

and the matrix coefficients have the following dimensions:
$A_i \in R^{p\times p}$, $B_i \in R^{p\times m}$, $C_i \in R^{m\times p}$ And $D_i \in R^{m\times m}$

3. Extended Least Squares Based on Left MFD

A MIMO ARX (Autoregressive with Exogenous Excitation) model is given by:

$$A(q^{-1})y[k] = B(q^{-1})u[k] + e[k] \tag{5}$$

which can be rewritten in Left MFD form as:

$$y[k] = A(q^{-1})^{-1}B(q^{-1})u[k] + A(q^{-1})^{-1}e[k] \tag{6}$$

where $u[k] \in R^m$ and $B_i \in R^{p\times m}$ are inputs and outputs vectors of the system respectively, while $e[k] \in R^p$ is a white-noise signal and the polynomial matrices $A^{-1}(q^{-1})$, $B(q^{-1})$ have the following structures:

$$A(q^{-1}) = I_p + A_1 q^{-1} + \cdots + A_{na} q^{-na} \tag{7}$$

$$B(q^{-1}) = B_1 q^{-1} + \cdots + B_{nb} q^{-nb} \tag{8}$$

The objective is to identify the matrix coefficients $A_i \in R^{p\times p}$ and $B_i \in R^{p\times m}$ of the matrix polynomials $C^{-1}(q^{-1}) = I_p$ and $B(q^{-1})$ assuming in this case that $C^{-1}(q^{-1}) = I_p$. Taking the transpose of Eq. (5) and expanding $A^{-1}(q^{-1})$ and $B(q^{-1})$, the following expressions are obtained:

$$\begin{aligned} e^T[k] &= \left(y^T[k] + y^T[k-1]A_1^T \cdots + y^T[k-na]A_{na}{}^T\right) - \left(u^T[k-1]B_1^T \cdots - u^T[k-nb]B_{nb}{}^T\right) \\ e^T[k] &= y^T[k] - \varphi^T[k]\theta \end{aligned} \tag{9}$$

where

$$\varphi^T[k] = [-y^T[k-1] \ldots - y^T[k-n_a], u^T[k-1] \ldots u^T[k-n_b]]$$

$$\theta = \left[A_1^T \cdots A_{na}{}^T, B_1^T \cdots B_{nb}{}^T\right]^T$$

The estimator is based on least squares, which is given as follows:

$$\hat{\theta}_{ls} = \left(\Phi^T\Phi\right)^{-1}\Phi^T Y \tag{10}$$

where, Y and Φ are functions of y and u, Hence:

$$Y = \begin{pmatrix} y^T[n+1,:] \\ \vdots \\ y^T[M,:] \end{pmatrix}, \ \Phi = \left(\Phi_y \vdots \Phi_u\right), \Phi_y = \begin{pmatrix} \begin{pmatrix} -y^T[n,:] \\ \vdots \\ -y^T[M-1,:] \end{pmatrix} & \cdots & \begin{pmatrix} -y^T[n-n_a+1,:] \\ \vdots \\ -y^T[M-n_a,:] \end{pmatrix} \end{pmatrix}$$

$$\Phi_u = \begin{pmatrix} \begin{pmatrix} u^T[n,:] \\ \vdots \\ u^T[M-1,:] \end{pmatrix} & \cdots & \begin{pmatrix} u^T[n-n_b+1,:] \\ \vdots \\ u^T[M-n_b,:] \end{pmatrix} \end{pmatrix} \tag{11}$$

where, n_a and M are the numbers of (Inputs/Outputs) data.

4. Hammerstein-Wiener Model Identification

A relatively simple way to represent the nonlinear behavior of a system based on the use of base models of structured blocks i.e. the combination of two basic blocks:

a nonlinear static element and a linear dynamic element. Among these models, there are the Hammerstein model, the Wiener model, the model of Wiener-Hammerstein, the Hammerstein-Wiener model [24]. The Hammerstein model presented in Fig. 1 (surrounded with blue), is composed of a nonlinear static element in cascade with a linear dynamic block. The input signal begins with the nonlinear static model to give the intermediate output signal, where itself is transformed by the linear dynamic part to give the output of the model. The non-linear element can explain the type of the actuator non-linearity and other effects that can be placed at the input of the model. Despite their simplicity, the Hammerstein models has been proved to have the ability to represent a large variety of nonlinear systems, for example, a chemical reactor, power amplifier, etc.

The permutation of linear and non-linear in the Hammerstein model leads to Wiener models. Its structure is shown in Fig. 1 (surrounded with green). Wiener models has been proved suitable for characterizing and using a linear model of the dynamic behavior of a system in which the sensor has a nonlinear character. The combination of a Hammerstein model and a model of Wiener, develops a new type of structure, Hammerstein-Wiener Fig. 1. A Wiener-Hammerstein model type can also be obtained on the same principle but in reverse order models. Hammerstein-Wiener models has been proved to be suitable for characterizing a system in which the actuator and sensor have a nonlinear character [25]. It has been successfully applied to the modelling of several industrial systems and process among them the turbo-compressor that is the subject of the study presented in this work.

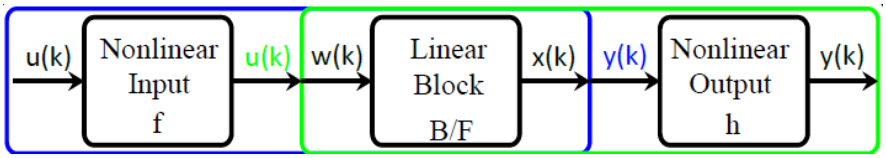

Fig. 1. Schematic block diagram of a Hammerstein-Wiener model.

In Fig. 1, the input data *u(k)* is transformed by a nonlinear function which yields to $w(k) = f(u(k))$, $w(k)$ is of the same size as $u(t)$ which is transformed once more to a linear function $x(k) = \frac{B}{F} w(k)$, where $x(t)$ is of the same size as $y(k)$, B and F are two linear polynomials in the output-error model, the transfer function matrix is a linear block of *ny* outputs and *nu* inputs containing entries:

$$\frac{B_{jj}(z)}{F_{jj}(z)}, \text{ where } j = 1,2,\ldots,ny \text{ and } i = 1,2,\ldots,nu. \tag{12}$$

the output of the system is obtained by: $y(k) = h(x(k))$ which has a nonlinear behaviour.

Furthermore $w(k)$ and $x(k)$ present the input/output of the linear block internal variables [34].

The Hammerstein-Wiener model calculates the output *y* in three steps:

a. Computes $w(k) = f(u(k))$ which presents the nonlinear input configured from the input data, it can take many functions forms as dead zone, saturation, wavelet network, sigmoid network, piecewise linear function, a custom network or one-dimensional polynomial.

b. Calculates the output of the linear block and using the initial conditions based on the signal $w(k)$: $x(k) = \frac{B}{F} w(k)$, the linear block configured by adjusting the numerator *B* /denominator *F* polynomials orders.
c. Transforms the output of the linear block $x(k)$ in order to compute the model output, using the nonlinear function *h:* $y(k) = h(x(k))$, Similar to the input nonlinearity, the output nonlinearity is a static function. The output nonlinearity can be configured in the same way as the input nonlinearity. Whereas, the output nonlinearity can be removed, such that $y(k) = x(k)$.

The model obtained with Hammerstein Wiener model can be written in the form of nonlinear State-space:

$$\begin{cases} x(k+1) = Ax(k) + Bu(k) + Ke(k) \\ y(k) = Cx(k) + Du(k) + e(k) \end{cases} \tag{13}$$

5. Model Validation

In literatures many important validations criteria can be found such as [26, 27]:

5.1. AIC

The Akaike Information Criterion for an estimated model:

$$AIC = Ln(V) + \frac{2d}{N} \tag{14}$$

V is the loss function, *d* is the number of estimated parameters and *N* is the number of samples in the estimation data set.

5.2. FPE

The Akaike's Final Prediction Error (FPE) is defined by:

$$FPE = V\left(\frac{1+\frac{d}{N}}{1-\frac{d}{N}}\right) \tag{15}$$

d and *N* are the same as in Eq. (14)

5.3. RMSE

The normalized root mean squared error, which is given by the following expression:

$$RMSE = \sqrt{\frac{\sum_{i=1}^{n}(y-\hat{y})^2}{N}} \tag{16}$$

5.4. VAF

Variance Accounting for (VAF) is defined as follows:

$$VAF = 100\%\left[1 - \frac{var(y-\hat{y})}{var(y)}\right] \tag{17}$$

The best system order *n* corresponding to minima of AIC, FPE, RMSE and maximum of VAF.

6. Application and Results

The system under study is a gas Turbo-compressor which is installed in Hassi R'mel Natural gas pumping station, it is composed of two inputs T1 and P1 (aspiration temperature and pressure) and two outputs T2 and P2 (discharge temperature and pressure), Fig. 2 shows the schematic bloc diagram of the inputs/outputs signals and the turbine which drives the studied compressor, and the internal detailed description with the fundamental components are shown in Fig. 3. The size of the real data obtained in site and which is used for the identification is 1208 samples taken along a duration of 1208 hour, this data is obtained by measurement on site based on many experiments.

6.1. Validation and numerical model

The parametric identification of the Left MIMO ARX model is obtained based on Extended Least Square estimator (LMFD_ARX**)** and (MFD) theory, where the model that has been selected must have an even order (2, 4, 6…) because each matrix block *q* have a dimension of 2×2. Table 1shown below clarifies the change of the orders n until the best one is reached. From the results shown in the Table 1, it can be concluded that the best model which fits the minima of AICs, FPEs, RMSEs, the maximum of VAF validations criteria, and the minimum loss function without Pole/Zero cancellation (left coprime) is the model shown in Table 1 (row 5) which has an order $n = 10$ with number of blocks $l = 5$ and the second model is presented in presented (row 6), The best model is the one which has an order $n = 12$ with number of blocks $l = 6$.

Table 1 Turbo-compressor system model orders with validations criteria respectively.

		LMFD ARX					Hammerstein-Wiener						
l	***n***	**Loss Fun**	**AIC**	**FPE**	**RMSE**	**VAF (%)**	**Loss Fun**	**AIC**	**FPE**	**RMSE**	**VAF (%)**	**Norm**	**Iterations**
1	**2**	**5.4385**	**1.7200**	**5.5826**	**1.7200**	**82.5000**	**8.1532**	**2.2610**	**9.5732**	**2.8534**	**56.7800**	**90.1462**	**20**
2	**4**	**1.9967**	**0.7445**	**2.1024**	**1.7200**	**85.9050**	**6.0217**	**2.1033**	**7.8760**	**1.7350**	**79.8000**	**53.0829**	**20**
3	**6**	**1.1045**	**0.1789**	**1.1923**	**1.7200**	**87.6550**	**4.1530**	**1.6401**	**5.1214**	**1.6531**	**81.1214**	**70.1324**	**20**
4	**8**	**1.0263**	**0.1319**	**1.1350**	**1.7200**	**87.7750**	**3.6337**	**1.6247**	**4.8489**	**1.4921**	**82.7300**	**85.4198**	**20**
5	**10**	**0.9927**	**0.1251**	**1.1242**	**1.7200**	**87.8050**	**1.6788**	**0.7503**	**2.1134**	**1.1786**	**85.4100**	**20.6605**	**20**
6	**12**	**0.9932**	**0.1420**	**1.1395**	**1.7200**	**87.0010**	**0.9541**	**0.3139**	**1.2984**	**0.9902**	**87.6550**	**16.1805**	**20**

The comparison study between the two models, the linear and the nonlinear models based on the validations criteria leads to the results shown in Table 1. From Fig. 4, 5, 8 and 9, it can be seen clearly that the two models are approximately equal, due to the absence effect of the nonlinearity phenomena in acquired data. Hence, the linear model is preferable to the nonlinear one, and the low order model (n=10) is more suitable to the model of the high order (n=12).

The selected model of the studied gas turbo-compressor system from the comparison study is a linear model, which is presented, in state space block observable canonical form, it is given as follow:

$$A=\begin{pmatrix} Z & Z & Z & Z & -A_5 \\ I & Z & Z & Z & -A_4 \\ Z & I & Z & Z & -A_3 \\ Z & Z & I & Z & -A_2 \\ Z & Z & Z & I & -A_1 \end{pmatrix},\ B=\begin{pmatrix} B_5 \\ B_4 \\ B_3 \\ B_2 \\ B_1 \end{pmatrix},\ C^T=\begin{pmatrix} Z \\ Z \\ Z \\ Z \\ I' \end{pmatrix},\ D=Z,\ I=\begin{pmatrix} 1 & 0 \\ 0 & 1 \end{pmatrix}\ Z=\begin{pmatrix} 0 & 0 \\ 0 & 0 \end{pmatrix}$$

yield,

$$A=\begin{pmatrix} 0 & 0 & 0 & 0 & 0 & 0 & 0 & 0 & -0.0152 & 0.0185 \\ 0 & 0 & 0 & 0 & 0 & 0 & 0 & 0 & 0.0389 & 0.0436 \\ 1 & 0 & 0 & 0 & 0 & 0 & 0 & 0 & 0.0666 & 0.0696 \\ 0 & 1 & 0 & 0 & 0 & 0 & 0 & 0 & 0.0881 & 0.1080 \\ 0 & 0 & 1 & 0 & 0 & 0 & 0 & 0 & 0.0959 & 0.0784 \\ 0 & 0 & 0 & 1 & 0 & 0 & 0 & 0 & 0.0508 & 0.0701 \\ 0 & 0 & 0 & 0 & 1 & 0 & 0 & 0 & -0.0171 & 0.0319 \\ 0 & 0 & 0 & 0 & 0 & 1 & 0 & 0 & 0.1294 & 0.0158 \\ 0 & 0 & 0 & 0 & 0 & 0 & 1 & 0 & -0.0052 & 0.0145 \\ 0 & 0 & 0 & 0 & 0 & 0 & 0 & 1 & 0.0699 & 0.0038 \end{pmatrix},\ B=\begin{pmatrix} 0.0245 & 0.0262 \\ 0.0686 & 0.0045 \\ 0.0219 & 0.0425 \\ 0.0199 & 0.0710 \\ 0.0820 & 0.2317 \\ 0.1615 & 0.1233 \\ 0.1762 & 0.0941 \\ 0.3274 & 0.1871 \\ 0.0857 & 0.2576 \\ -0.0801 & -0.0413 \end{pmatrix},\ C^T=\begin{pmatrix} 0 & 0 \\ 0 & 0 \\ 0 & 0 \\ 0 & 0 \\ 0 & 0 \\ 0 & 0 \\ 0 & 0 \\ 0 & 0 \\ 1 & 0 \\ 0 & 1 \end{pmatrix}$$

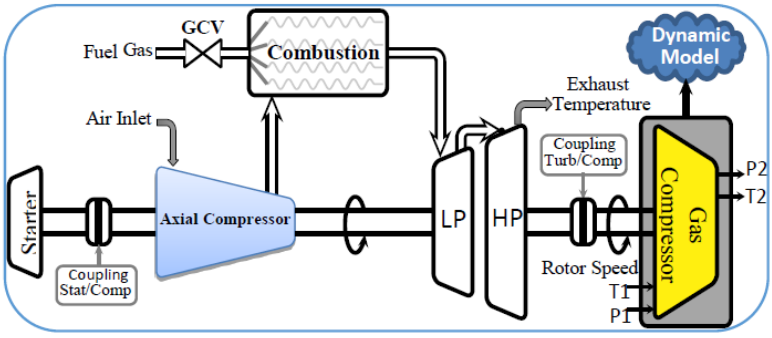

Fig. 2. Schematic bloc diagram of gas turbo-compressor with inputs/outputs model identification.

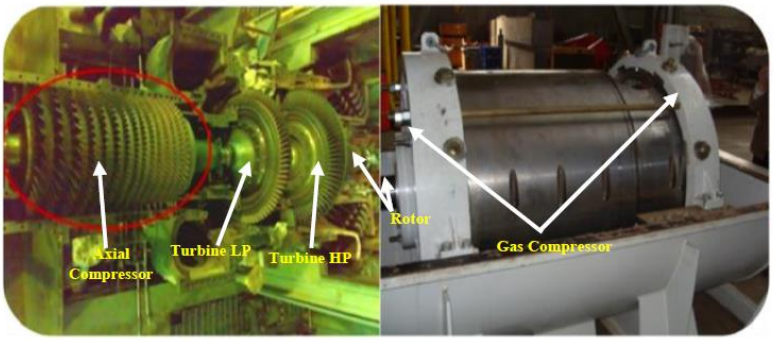

Fig. 3. The studied gas turbo-compressor, internal viewing with detailed description of their fundamental components.

6.2. Inputs outputs and error signals

Through the measured and the estimated outputs signals shown in Figs. 4 and 5, it can be seen clearly that the estimated discharge Pressure P2 tracks the measured along the time of measurement, from 0 kg/cm2 up to 100 kg/cm^2 during 40 hours. The same thing is obtained for the estimated discharge Temperature T2 which tracks the measured signal, from 0 °C up to 120 °C during 50 hours. Figure 6 represents the signal input T1, where variation of the aspiration temperature is shown from 58 °C up to 65 °C, and Fig. 7 represents the aspiration pressure (P1) variation from 55 kg/cm2 up to 68 kg/cm^2. The outputs errors signal validation shown in Figs. 8 and 9, it is clear that the signal error of discharge pressure is bounded between ± 2.5 kg/cm^2, and converges when the time reaches it maximum, the signal error of discharge temperature is bounded between ± 2.5 °C, where it converges.

The effects of aging or failure of mechanical components in dynamical systems through time appear randomly. Indeed; in the field of turbo-machinery, especially in turbo-compressor where the loss in modelling phenomena due to the degradation in the components and also the difficult climatic conditions in the desert which affect the dynamics of this system. Thus, the stability and the performance robustness of the obtained dynamical model of the turbo-compressor under structural uncertainties have been analysed using zero-pole map analysis method in order to measure the robustness of the obtained model against the uncertainties. The system under the injection of the 10% uncertainty to the nominal model the pole-zero map in Fig. 10 shows that the system maintains all-important keys where the real part of the poles rest in the left half plan and the system controllability and observability are also maintains, this study shows that the robustness of the proposed model is well suitable.

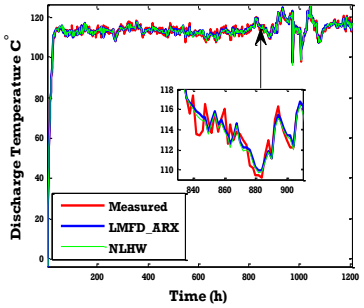

Fig. 4. Outputs signals of estimated/ measure discharge Temperature.

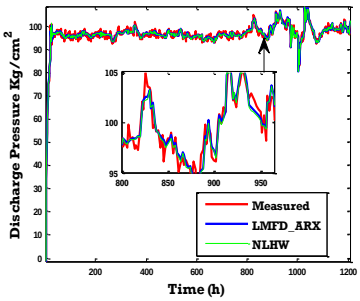

Fig. 5. Outputs signals of estimated/ measured discharge pressure.

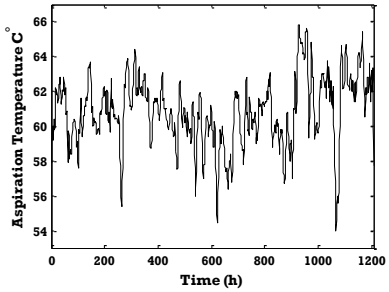

Fig. 6. Input signal of aspiration temperature.

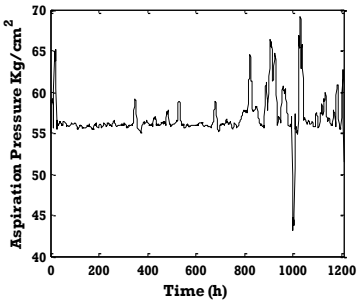

Fig. 7. Input signal of aspiration pressure.

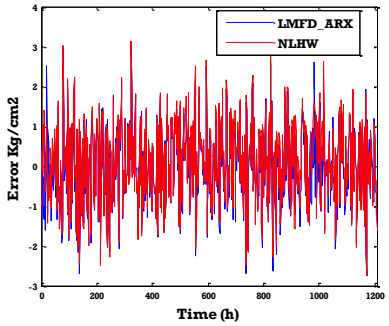

Fig. 8. Error signal of measured / estimated discharge pressure.

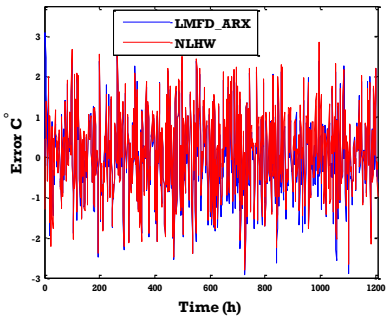

Fig. 9. Error signal of measured/ discharge temperature.

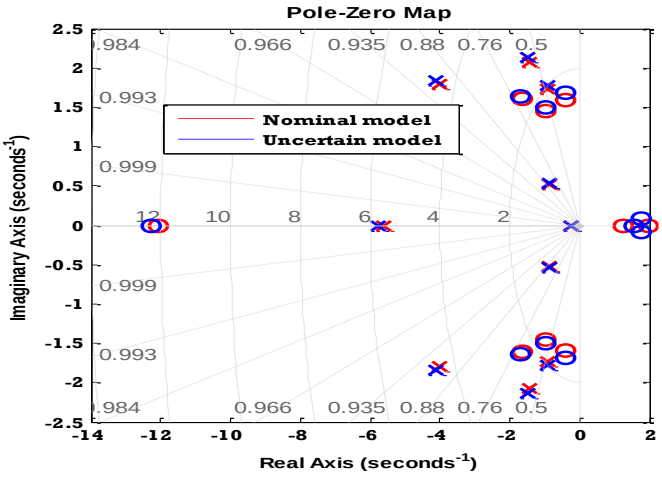

Fig. 10. Pole-zero map of the nominal and the uncertain model of the turbo-compressor system.

7. Block Solvents Assignment Dynamic Control

This algorithm is an extension of classical pole placement using the theory of matrix fraction description, this numerical application gives the necessary steps and results without equations [28, 29].

Consider the system, which is described by the following dynamic equation:

$$\begin{cases} \dot{x}(t) = Ax(t) + Bu(t) \\ y(t) = Cx(t) + Du(t) \end{cases} \tag{18}$$

where, $A \in R^{n\times n}$, $B \in R^{n\times m}$, $C \in R^{p\times n}$ and $D \in R^{p\times m}$, n=10, m=2and p=2.

The system can be transformed to a block controllable form, where:

- The number $\frac{n}{m} = l = \frac{10}{2} = 5$ is an integer.
- The matrix $W_c = \left(A\ AB\ A^2B\ A^3B\ A^4B\right)$ is of full rank 10.

$$T_c = \begin{pmatrix} T_{cl} \\ T_{cl}A^1 \\ T_{cl}A^2 \\ T_{cl}A^3 \\ T_{cl}A^4 \end{pmatrix}, \; T_{cl} = \begin{pmatrix} Z & Z & Z & Z & I \end{pmatrix}\begin{pmatrix} B & AB & A^2B & A^3B & A^4B \end{pmatrix}^{-1}$$

The new system becomes:

$$\begin{cases} \dot{x}(t) = A_c x(t) + B_c u(t) \\ y(t) = C_c x(t) \end{cases}$$

with, $A_c = T_c A T_c^{-1}, \quad B_c = T_c B, \quad C_c = C T_c^{-1}$

$$A_c = \begin{pmatrix} Z & I & Z & Z & Z \\ Z & Z & I & Z & Z \\ Z & Z & Z & I & Z \\ Z & Z & Z & Z & I \\ -Ac_5 & -Ac_4 & -Ac_3 & -Ac_2 & -Ac_1 \end{pmatrix}, \; B_c = \begin{pmatrix} Z \\ Z \\ Z \\ Z \\ I \end{pmatrix}, \; C_c = \begin{pmatrix} Cc_5 & Cc_4 & Cc_3 & Cc_2 & Cc_1 \end{pmatrix}$$

where,

$$Ac_1 = \begin{pmatrix} -4.4447 & 3.9169 \\ -12.6792 & -15.7734 \end{pmatrix}, \quad Ac_2 = \begin{pmatrix} 15.4001 & 34.8676 \\ -106.9661 & -75.4377 \end{pmatrix}, \quad Ac_3 = \begin{pmatrix} 138.4403 & 116.2885 \\ -255.8348 & -125.7872 \end{pmatrix}$$

$$Ac_4 = \begin{pmatrix} 262.4191 & 133.4632 \\ -248.7160 & -96.1883 \end{pmatrix}, \quad Ac_5 = \begin{pmatrix} 112.8116 & 38.7745 \\ -101.0696 & -29.5472 \end{pmatrix}, \quad Cc_1 = \begin{pmatrix} 0.0556 & 2.8720 \\ 0.0274 & -0.7992 \end{pmatrix}$$

$$Cc_2 = \begin{pmatrix} 33.8989 & 28.2277 \\ -21.853 & -11.3608 \end{pmatrix}, \quad Cc_3 = \begin{pmatrix} 105.8492 & 54.7677 \\ -19.2074 & 11.5656 \end{pmatrix}, \quad Cc_4 = \begin{pmatrix} 122.0492 & 49.0349 \\ 48.6800 & 21.1917 \end{pmatrix}$$

$$Cc_5 = \begin{pmatrix} 58.5562 & 13.1484 \\ -10.6175 & -7.7350 \end{pmatrix}, \quad Cc_3 = \begin{pmatrix} 105.8492 & 54.7677 \\ -19.2074 & 11.5656 \end{pmatrix}, \quad Cc_4 = \begin{pmatrix} 122.0492 & 49.0349 \\ 48.6800 & 21.1917 \end{pmatrix}$$

$$Cc_5 = \begin{pmatrix} 58.5562 & 13.1484 \\ -10.6175 & -7.7350 \end{pmatrix}, \quad I = \begin{pmatrix} 1 & 0 \\ 0 & 1 \end{pmatrix}, \quad Z = \begin{pmatrix} 0 & 0 \\ 0 & 0 \end{pmatrix}$$

- Block Solvents in diagonal form

$$S_1 = \begin{pmatrix} -.5 & 0 \\ 0 & -.2 \end{pmatrix}, S_2 = \begin{pmatrix} -.35 & 0 \\ 0 & -1 \end{pmatrix}, S_3 = \begin{pmatrix} -.75 & 0 \\ 0 & -.65 \end{pmatrix}, S_4 = \begin{pmatrix} -.07 & 0 \\ 0 & -.09 \end{pmatrix}, \; S_5 = \begin{pmatrix} -.8 & 0 \\ 0 & -1.5 \end{pmatrix}$$

- Block Solvents in controllable form

$$S_1 = \begin{pmatrix} -.7 & -.1 \\ 1 & 0 \end{pmatrix}, S_2 = \begin{pmatrix} -1.35 & -.35 \\ 1 & 0 \end{pmatrix}, S_3 = \begin{pmatrix} -1.4 & -0.48 \\ 1 & 0 \end{pmatrix}, S_4 = \begin{pmatrix} 0 & 1 \\ -0.063 & -0.79 \end{pmatrix}, S_5 = \begin{pmatrix} 0 & 1 \\ -1.2 & -2.3 \end{pmatrix}$$

- Block Solvents in observable form

$$S_1 = \begin{pmatrix} 0 & -.1 \\ 1 & -.7 \end{pmatrix}, S_2 = \begin{pmatrix} 0 & -.35 \\ 1 & -1.35 \end{pmatrix}, S_3 = \begin{pmatrix} 0 & -0.487 \\ 1 & -1.4 \end{pmatrix}, S_4 = \begin{pmatrix} 0 & -0.063 \\ 1 & -0.79 \end{pmatrix}, S_5 = \begin{pmatrix} 0 & -1.2 \\ 1 & -2.3 \end{pmatrix}$$

7.1. Constructing right block solvents:

Consider a complete set of right solvents $\{S_1, S_2, S_3, S_4, S_5\}$ for the matrix polynomial $D(\lambda)$, If S_i is a right solvent of $D(\lambda)$ so:

$$\begin{cases} S_i^5 + D_1 S_i^4 + D_2 S_i^3 + D_3 S_i^2 + D_4 S_i + D_5 = Z \\ \Leftrightarrow \\ D_1 S_i^4 + D_2 S_i^3 + D_3 S_i^2 + D_4 S_i + D_5 = -S_i^5 \end{cases}$$

Replacing *i* from 1 to 5, yields to:

$$\left(D_{d5}\ D_{d4}\ D_{d3}\ D_{d2}\ D_{d1}\right) = -\left(S_1^5\ S_2^5\ S_3^5\ S_4^5\ S_5^5\right) V_R^{-1}$$

where V_R is the right block Vandermonde matrix.

$$V_R = \begin{pmatrix} I & I & I & I & I \\ S_1^1 & S_2^1 & S_3^1 & S_4^1 & S_5^1 \\ S_1^2 & S_2^2 & S_3^2 & S_4^2 & S_5^2 \\ S_1^3 & S_2^3 & S_3^3 & S_4^3 & S_5^3 \\ S_1^4 & S_2^4 & S_3^4 & S_4^4 & S_5^4 \end{pmatrix}$$

7.2. Constructing left block solvents

Consider a complete set of left solvents $\{S_1, S_2, S_3, S_4, S_5\}$ for the matrix polynomial $D(\lambda)$ If S_i is a left solvent of $D(\lambda)$ so:

$$\begin{cases} S_i^5 + S_i^4 D_1 + S_i^3 D_2 + S_i^2 D_3 + S_i D_4 + D_5 = Z \\ \Leftrightarrow \\ S_i^4 D_1 + S_i^3 D_2 + S_i^2 D_3 + S_i D_4 + D_5 = -S_i^5 \end{cases}$$

Replacing i from 1 to 5, yields to:

$$\begin{pmatrix} D_{d5} \\ D_{d4} \\ D_{d3} \\ D_{d2} \\ D_{d1} \end{pmatrix} = -V_L^{-1} \begin{pmatrix} S_1^5 \\ S_2^5 \\ S_3^5 \\ S_4^5 \\ S_5^5 \end{pmatrix}$$, where V_L is the left block Vandermonde matrix.

and

$$V_L = \begin{pmatrix} I & S_1 & S_1^2 & S_1^3 & S_1^4 \\ I & S_2 & S_2^2 & S_2^3 & S_2^4 \\ I & S_3 & S_3^2 & S_3^3 & S_3^4 \\ I & S_4 & S_4^2 & S_4^3 & S_4^4 \\ I & S_5 & S_5^2 & S_5^3 & S_5^4 \end{pmatrix}$$

7.3. State Feedback matrix gain

Consider the linear system of turbo-compressor described by Eq. (21), the state feedback $u = -Kx(t)$, K is a 2×10 gain matrix, after the transformation into the block controllable form, the following expression is obtained:

$u = K_c x_c(t)$.

$K = K_c T_c = \left(K_{c(5)}, K_{c(4)}, K_{c(3)}, K_{c(2)}, K_{c(1)}\right)$

T_c and $K_{ci} \in R^{m \times m}$ For i = 1...,5, the closed loop system is shown below:

$$\begin{cases} \dot{x}_c = \left(A_c - B_c K_c\right) x_c \\ y_c = C_c x_c \end{cases}$$

where,

$$\left(A_c - B_c K_c\right) = \begin{pmatrix} Z & I & Z & Z & Z \\ Z & Z & I & Z & Z \\ Z & Z & Z & I & Z \\ Z & Z & Z & Z & I \\ -\left(A_5 + K_{c5}\right) & -\left(A_4 + K_{c4}\right) & -\left(A_3 + K_{c3}\right) & -\left(A_2 + K_{c2}\right) & -\left(A_1 + K_{c1}\right) \end{pmatrix}$$

The characteristic matrix polynomial of this closed loop system is:

$$D(\lambda) = I\lambda^5 + \left(A_1 + K_{c1}\right)\lambda^4 + \ldots + \left(A_5 + K_{c5}\right)$$

From a set of desired eigenvalues, the set of Block poles can be constructed. The desired characteristic matrix polynomial of the block poles in the right form, by putting, $D_d(\lambda) = D(\lambda)$. The coefficients $K_{ci} = D_{di} - A_i$ are obtained as follows:

Feedback Static Gain Matrix in right diagonal form

$$K = \begin{pmatrix} 45.5831 & -28.8103 & 28.3961 & -10.1292 & -16.6398 & 11.9460 & -7.0725 & -3.8599 & 9.7949 & 0.9209 \\ 38.5295 & -42.7067 & -57.2365 & 56.3219 & -10.9989 & -19.9014 & 31.8083 & 2.9674 & -12.7137 & -0.9948 \end{pmatrix}$$

Feedback Static Gain Matrix in right controllable form

$$K = \begin{pmatrix} 14.2953 & -15.3840 & 31.4307 & -13.2777 & -9.2161 & 8.6137 & -10.0276 & -2.3323 & 8.1703 & 0.9247 \\ 59.0194 & -52.2588 & -64.2053 & 62.1368 & -14.8935 & -19.7696 & 35.4016 & 2.2845 & -12.7636 & -0.9837 \end{pmatrix}$$

Feedback Static Gain Matrix in right observable form

$$K = \begin{pmatrix} -78.6152 & 22.2683 & 39.6588 & -20.6924 & 12.3512 & -0.7257 & -17.7800 & 2.2566 & 2.7699 & 0.3594 \\ -136.057 & 29.0071 & -42.2787 & 42.1001 & 29.9653 & -38.569 & 16.9891 & 11.740 & -22.726 & -1.6352 \end{pmatrix}$$

Feedback Static Gain Matrix in left diagonal form

$$K = \begin{pmatrix} 45.5831 & -28.8103 & 28.3961 & -10.1292 & -16.6398 & 11.9460 & -7.0725 & -3.8599 & 9.7949 & 0.9209 \\ 38.5295 & -42.7067 & -57.2365 & 56.3219 & -10.9989 & -19.9014 & 31.8083 & 2.9674 & -12.7137 & -0.9948 \end{pmatrix}$$

Feedback Static Gain Matrix in left controllable form

$$K = \begin{pmatrix} -227.3410 & 126.3244 & -238.8049 & 141.9400 & 125.2135 & -98.0163 & 45.1448 & 7.6374 & -64.5548 & 1.5484 \\ 267.1105 & -180.6756 & 207.6107 & -95.6571 & -141.1419 & 82.8652 & -22.4126 & -5.7331 & 57.8859 & -1.6456 \end{pmatrix}$$

Feedback Static Gain Matrix in left observable form

$$K = \begin{pmatrix} -6.1938 & -0.6851 & 9.7471 & -1.9941 & 2.4590 & 1.8022 & -6.1898 & -2.3837 & 2.3253 & 0.7784 \\ 30.3769 & -36.0879 & -67.4850 & 61.5009 & -5.7573 & -23.3141 & 33.5945 & 2.9327 & -15.2838 & -0.9022 \end{pmatrix}$$

8. Discussion

Based on the results shown in Tables 1, 2, 3 and 4 it can be concluded that:

a. From Table 2 which represents different norms of different feedback static matrix gain it can be said that:
- The observable block solvents in the left is enough.
- The diagonal block solvents left/right are equals and more enough.
- The controllable block solvents in the right is enough.
- The right/left observable/controllable block solvents respectively are not suitable.

These provisions are not sufficient to determine the optimal controller so the results obtained in Table 3 has to be checked.

b. From the Table 3 which represents the time specifications of different feedback static matrix gain, it can be said that:
- The left and the right of the observable block solvents form give bad results and this form is not valid in this study.
- The right controllable block solvents form is more suitable then left in all the time specifications.
- The left/ right diagonal block solvents form gives the same results and are enough.

Based on the discussion of the results and from the comparative study shown in the Table 4, the static feedback matrix gain of the right controllable block solvents form is the best and where the stability is ensured by the controller, because it collects the high performance, best time specifications results with minimum and reasonable consumption of energy control.

Table 2. The norms (1, 2, inf and fro) of feedback matrix gain *K*.

		$\|K\|_1$	$\|K\|_2$	$\|K\|_{inf}$	$\|K\|_{fro}$
Diagonal Block Solvents	Right	85.6326	107.1288	274.1790	125.9162
	Left	85.6326	107.1288	274.1790	125.9162
Controllable Block Solvents	Right	95.6360	128.1819	323.7167	181.2496
	Left	494.4515	599.1810	1.0765e+3	602.7345
Observable Block Solvents	Right	214.6730	173.2175	371.0688	150.8790
	Left	77.2321	112.4092	277.2353	112.7257

Table 3. Time specifications of the two outputs affected by the inputs.

			Diagonal form		Controllable form		Observable form	
			Right	Left	Right	Left	Right	Left
T1	P2	Rise Time	10.0206	10.0206	7.9990	23.9312	26.6525	14.8913
		Settling Time	17.4065	17.4065	12.4987	46.4843	62.3504	38.1158
		Settling Min	718.1322	718.1322	694.6842	2.7623e+4	339.0753	-173.7579

	Settling Max	796.6862	796.6862	784.9853	3.0684e+4	376.4863	-156.6178
	Over shoot	1.9196e-9	0	1.8657	0	0	0
	Under shoot	0	0	0	0	34.7490	121.6249
	Peak	796.6862	796.6862	784.9853	3.0684e+4	376.4863	211.5268
	Peak Time	85.9621	85.9621	17.8359	107.8399	105.5467	7.1828
T2	Rise Time	8.6857	8.6857	13.2644	22.6812	67.2990	32.2554
T2	Settling Time	21.8839	21.8839	29.9263	52.3163	68.7731	46.8101
T2	Settling Min	-144.2570	-144.2570	-453.1357	-2.3814e+3	-22.2499	92.2824
T2	Settling Max	-130.0222	-130.0222	-408.1791	-2.1448e+3	-20.0949	102.3481
T2	Over shoot	8.2295e-9	0	0	0	0	0
T2	Under shoot	24.3631	24.3631	11.0453	23.1327	496.2182	39.8958
T2	Peak	144.2570	144.2570	453.1357	2.3814e+3	110.8922	102.3481
T2	Peak Time	85.9621	85.9621	83.8530	107.8399	17.9059	77.3966
P1 P2	Rise Time	27.8101	27.8101	23.8351	25.6268	23.0097	15.5562
P1 P2	Settling Time	49.4637	49.4637	54.7473	48.8321	44.1733	28.2406
P1 P2	Settling Min	674.0113	674.0113	-126.0195	3.1809e+4	2.4089e+3	3.6767e+3
P1 P2	Settling Max	748.2657	748.2657	-113.9484	3.5324e+4	2.6753e+3	4.0799e+3
P1 P2	Over shoot	0	0	0	0	0	0
P1 P2	Under shoot	0.0495	0.0495	150.6509	0.0010	0.0139	0.0091
P1 P2	Peak	748.2657	748.2657	190.5437	3.5324e+4	2.6753e+3	4.0799e+3
P1 P2	Peak Time	85.9621	85.9621	8.6355	107.8399	105.5467	77.3966
P1 T2	Rise Time	27.8615	27.8615	9.4850	24.3230	22.0021	14.4579
P1 T2	Settling Time	55.3850	55.3850	42.0721	54.8745	48.3289	33.1389
P1 T2	Settling Min	-440.0054	-440.0054	-251.6543	-2.7495e+3	-804.7499	-1.0036e+3
P1 T2	Settling Max	-396.6555	-396.6555	-216.8959	-2.4763e+3	-724.5549	-903.5474
P1 T2	Over shoot	0	0	4.4752	0	0	0
P1 T2	Under shoot	3.9441	3.9441	10.2244	20.4546	7.2138	8.3428
P1 T2	Peak	440.0054	440.0054	251.6543	2.7495e+3	804.7499	1.0036e+3
P1 T2	Peak Time	85.9621	85.9621	28.7312	107.8399	105.5467	77.3966

Table 4. Comparative study results.

		Diagonal form		Controllable form		Observable form	
		Right	Left	Right	Left	Right	Left
The norms	$\|K\|_1$	Right = Left		Right		Left	
The norms	$\|K\|_2$	Right = Left		Right		Left	
The norms	$\|K\|_{inf}$	Right = Left		Right		Left	
The norms	$\|K\|_{fro}$	Right = Left		Right		Left	
Time specifications	Rise Time	Right = Left		Right		Left	
Time specifications	Settling Time	Right = Left		Right		Left	
Time specifications	Settling Min	Right = Left		Right		Right	
Time specifications	Settling Max	Right = Left		Right		Right	
Time specifications	Over shoot	Right = Left		Right = Left		Right = Left	
Time specifications	Under shoot	Right = Left		Right = Left		Right = Left	
Time specifications	Peak	Right = Left		Right		Right = Left	
Time specifications	Peak Time	Right = Left		Right		Right = Left	

9. Conclusions

In this paper, the application of the Left Matrix Fraction Description (LMFD) theory is proposed for the parametric identification of a turbo-compressor driven by a gas turbine, which is used, in an important power plant. Indeed, this system presents a high dimension ARX model; where the application of the LMFD in such

case in proposed here in this paper for the first time as a new original work. Furthermore, this proposed parametric identification is based on real (inputs/outputs) data that have been measured on-site, where the extended least square (ELS) estimator due to its main merits, such as the reliability (unbiased estimator in this case) compared with the recursive estimators, the ease implementation due to its simple mathematical structure and the richness of the data versus the frequency, this last allows facilitating the design of the estimator.

For the validation of the obtained dynamical model and its robustness, four testing criteria are used such as the two robust criteria (AIC and FPE) and two other criteria (RMSE and VAF), where the main objective is to achieve the selection requirement of the best model order without Pole/Zero cancellation (left coprime). On the other side, the Hammerstein-Wiener model identification is used as comparative model based on the obtained reliability. Finally, in order to improve the stability of the studied system which is used in a very vital and sensible power plant for ensuring the transporting the natural gas under high pressure, the block solvents placement based on MFD theory is proposed in different forms to make the dynamic behaviour of the turbo-compressor more stable. As a perspective for the present work, is the implementation of the dynamic model proposed in this paper on the diagnostics and fault tolerant control applications of the studied system.

Acknowledgments

Our sincere thanks the Staff (administrator's professionals and technicians) of north zone (north compression station) in Hassi R'mel Gas Field, Algeria, for all those helped to complete this work and overcome the difficulties encountered.

References

1. Pourfarzaneh, H.; Hajilouy-Benisi, A.; and Farshchi, M. (2010). A new analytical model of a centrifugal compressor and validation by experiments. *Journal of Mechanics*, 26(01), 37-45.
2. Bourgeois, J.A.; Martinuzzi, R.J.; Savory, E.; Zhang, C.; and Roberts, D.A. (2011). Assessment of turbulence model predictions for an aero-engine centrifugal compressor. *Journal of Turbomachinery*, 133(01), 1-15.
3. Munari, E.; Morini, M.; Pinelli, M.; Brun, K.; Simons, S.; and Kurz, R. (2017). Measurement and prediction of centrifugal compressor axial forces during surge: Part 2: Dynamic surge model. *Journal of Engineering for Gas Turbines and Power*, 9(1), 1-17.
4. Moore, J.J.; and Ransom, D.L. (2010). Centrifugal compressor stability prediction using a new physics based approach. *Journal of Engineering for Gas Turbines and Power*, 132(8), 1-8.
5. Brun, K.; and Kurz, R. (2010). Analysis of the effects of pulsations on the operational stability of centrifugal compressors in mixed reciprocating and centrifugal compressor stations. *Journal of Engineering for Gas Turbines and Power*, 132(7), 1-10.
6. Zhao, D.; Blunier, B.; Gao, F.; Dou, M.; and Miraoui, A. (2014). Control of an ultrahigh-speed centrifugal compressor for the air management of fuel cell systems. *IEEE Transactions on Industry Applications*, 50(3), 2225-2234.

7. Yang, M.; Zheng, X.; Zhang, Y.; Bamba, T.; Tamaki, H.; Huenteler, J.; and Li, Z. (2012). Stability improvement of high-pressure-ratio turbocharger centrifugal compressor by asymmetric flow control - Part I: Non-axisymmetrical flow in centrifugal compressor. *Journal of Turbomachinery*, 135(2), 1-8.
8. Bidaut, Y.; and Baumann, U. (2011). Improving the design of a high pressure casing with the help of finite element analysis to ensure the rotor dynamic stability of a high pressure centrifugal compressor equipped with a hole pattern seal. *Journal of Engineering for Gas Turbines and Power*, 133(7), 1-8.
9. Abdelhafid, B.; Ahmed, H.; and Mouloud, G. (2016). Gas turbine modelling based on fuzzy clustering algorithm using experimental data. *Journal of Applied Artificial Intelligence Taylor & Francis*, 30(1), 29-51.
10. Hafaifa, A.; Guemana, M.; and Belhadef, R. (2015). Fuzzy modelling and control of centrifugal compressor used in gas pipelines systems. multi physics modelling and simulation for systems design and monitoring. chapter. *Applied Condition Monitoring*, 2, 379-389.
11. Laaouad, F.; Fekhar, H.; and Hafaifa, A. (2002). Modeling centrifugal compressor using fuzzy logic. XVI. *International Conference on Thermodynamic. Saint-Petersburg*, Russia, July, 1-6.
12. Laaouad, F.; Fekhar, H.; and Hafaifa, A. (2002). Adaptive control of centrifugal compressors. *15th International Congress of Chemical and Process Engineering*, Prague, Czech Republic, 1-6.
13. Djaidir, B.; Hafaifa, A.; and Kouzou, A. (2015). Monitoring gas turbines using speedtronic mark vi control systems. *Pipeline & Gas Journal*, 242(10), 48-86.
14. Balamurugan, S.; Joseph, R.X.; and Ebenezer, A.J. (2008). Application of genetic algorithm in optimal PID gain tuning for heavy duty gas turbine plant. *J. Electrical Systems*, 4(4), 1-10.
15. Akroum, M.; and Hariche, K. (2008). An optimal instrumental variable identification method for LMFD models. *Journal of studies in informatics and control*, 17(4), 361-372.
16. Akroum, M.; and Hariche, K. (2009). Extending the SRIV algorithm to LMFD models. *Journal of electrical engineering and technology Korean Institute of electrical engineers*, 4(1), 135-142.
17. Al-Muthairi, N.F.; Bingulac, S.; and Zribi, M. (2002). Identification of discrete-time MIMO systems using a class of observable canonical-form. *IEEE Proc-Control Theory*, 149(2), 125-130.
18. Johansson, R. (1995). Multivariable system identification via continued-fraction approximation. *IEEE Transactions on Automatic Control*, 40(3), 507-512.
19. Guidorzi, R. (1975). Canonical structures in the identification of multivariable systems. *Automatica*, 11(4), 361-374.
20. Ding, F.; and Chen, T. (2005). Identification of Hammerstein non-linear ARMAX systems. *Automatica*, 41(9), 1479-1489.
21. Schoukens, R.M.; Pintelon; and Rolain, Y. (2011). Parametric identification of parallel Hammerstein systems. *IEEE Transactions on Instrumentation and Measurement*, 60(12), 3931- 3938.

22. Paduart, J.; Lauwers, L.; Pintelon, R.; and Schoukens, J. (2012). Identification of a Wiener Hammerstein system using the polynomial nonlinear state space approach. *Control Engineering Practice*, 20(11), 1133-1139.
23. Er-Wei, B. (2002). A blind approach to the Hammerstein Wiener model identification. *Automatica*, 38(6), 967-979.
24. Hammar, K.; Djamah, T.; and Bettayeb, M. (2015). Fractional Hammerstein system identification using polynomial non-linear state space model. *3rd International Conference on Control, Engineering & Information Technology*, Tlemcen, Algeria, 1-6.
25. Serssour, L.; Djamah, T.; Hammar, K.; and Bettayeb, M. (2015). Wiener system identification using polynomial non linear state space model. *3rd* International *Conference on Control, Engineering & Information Technology*, Tlemcen, Algeria, 1-6.
26. Ljung, L. (1999). *System identification: Theory for the user* (2nd ed.). USA: Prentice Hall.
27. Ljung, L. (2005). *System identification toolbox for MATLAB* (Version, 6.1.2.). USA: math-works.
28. Nail, B.; Kouzou, A.; and Hafaifa, A. (2016). Block Pole Assignment stabilization in large scale systems application to gas turbine power plant. *International Conference on Technological Advances in Electrical Engineering*, Skikda, Algeria, 1-6.
29. Hadroug, N.; Hafaifa, A.; Kouzou, A.; and Chaibet, A. (2017). Dynamic model linearization of two shafts gas turbine via their input/output data around the equilibrium points. *Energy*, 120(2), 488-497.
30. Kailath, T.; and Li, W. (1980). *Linear systems*. USA: Prentice Hall.
31. Shieh, L.S.; and Tsay, Y.T. (1982). Transformation of a class of multivariable control systems to Block companion forms. *IEEE Truns. Autonwt. Control*, 27(1), 199-203.
32. Bekhiti, B.; Dahimene, A.; Nail, B.; Hariche, K.; and Hamadouche, A. (2015). On block roots of matrix polynomials based mimo control system design. *4-th IEEE International Conference on Electrical Engineering, ICEE*, Boumerdes, Algeria, 1-6.
33. Gohberg, I.; Lancaster, P.; and Rodman, L. (2009). *Matrix polynomials*, Philadelphia: Society for Industrial and Applied Mathematics.
34. Hadroug, N.; Hafaifa, A.; Kouzou, A.; Guemana, M.; and Chaibet, A. (2016). Control of the speed and exhaust gas temperature in gas turbine using adaptive neuro-fuzzy inference system. *Journal of Automation & Systems Engineering*, 10(3), 158-167.